

Spin dynamics in the t - t' - J model: Dynamical density-matrix renormalization group study

Takami Tohyama,^{1,*} Shigetoshi Sota,² and Seiji Yunoki^{2,3,4}

¹*Department of Applied Physics, Tokyo University of Science, Tokyo 125-8585, Japan*

²*Computational Materials Science Research Team,*

RIKEN Center for Computational Science (R-CCS), Kobe, Hyogo 650-0047, Japan

³*Computational Condensed Matter Physics Laboratory,*

RIKEN Cluster for Pioneering Research (CPR), Wako, Saitama 351-0198, Japan

⁴*Computational Quantum Matter Research Team,*

RIKEN Center for Emergent Matter Science (CEMS), Wako, Saitama 351-0198, Japan

(Dated: June 16, 2022)

The ground state of a hole-doped t - t' - J ladder with four legs favors a striped charge distribution. Spin excitation from the striped ground state is known to exhibit incommensurate spin excitation near $\mathbf{q} = (\pi, \pi)$ forming an hourglass behavior along the leg direction (q_x direction). However, an outward dispersion from the incommensurate position toward $\mathbf{q} = (0, \pi)$ is strong in intensity, inconsistent with inelastic neutron scattering (INS) experiment. To clarify the origin of this inconsistency, we investigate the dynamical spin structure factor of n -leg t - t' - J ladder by using the dynamical density matrix renormalization group. With increasing $n = 4$ to $n = 8$, we find that the outward dispersion becomes weaker accompanied with weakening of stripe order in the ground state. In addition, excitation energy at $\mathbf{q} = (\pi, \pi)$ decreases with increasing n . The $n = 8$ results are closer to INS data in hole-doped cuprates than the $n = 4$ case. For understanding an direction dependent spin excitation reported by recent resonant inelastic x-ray scattering (RIXS) for cuprate superconductors, we also examine an 8×8 t - t' - J square lattice and obtain a consistent result with RIXS.

I. INTRODUCTION

In hole-doped cuprate superconductors, an hourglass-type spin excitation centered at the magnetic zone center in the Brillouin zone has been observed by inelastic neutron scattering (INS) experiment [1]. One of possible origins of the hourglass-type excitation is the formation of charge stripes in hole-doped cuprates [2] as discussed based on a two-dimensional (2D) single-band Hubbard model [3–5] and a localized spin model [6, 7]. Recent quantum Monte Carlo (QMC) calculations of the dynamical spin structure factor for a four-leg, three-band Hubbard ladder including oxygen orbitals [8] and for a t - t' - U four-leg ladder [9] have also indicated the hourglass-type excitation in the presence of the charge stripes where periodical arrangement of a river of charge on rung is formed along the leg direction.

A hole-doped four-leg t - t' - J ladder has also shown the charge-stripe ground state [10–13] and clear incommensurate spin excitation near the magnetic zone center at $\mathbf{q} = (\pi, \pi)$ forming an hourglass behavior as demonstrated by using the dynamical version of the density-matrix renormalization group (DMRG) [14]. The hourglass behavior qualitatively agrees with the experimental data when one uses ladders with four legs, but the presence of an outward dispersion with strong spectral weight from the incommensurate position toward $\mathbf{q} = (0, \pi)$ [14] is inconsistent with experimental observations [1]. The calculated energy of the $\mathbf{q} = (\pi, \pi)$ excitation is nearly

the same as the value of antiferromagnetic exchange interaction J [14], being also inconsistent with experimental observation showing less than half of J [1]. It is therefore crucially important to clarify the origin of these inconsistencies.

The number of hole carrier changes spin excitation in cuprates. Recent measurements of spin excitation in $\text{La}_{2-x}\text{Sr}_x\text{CuO}_4$ by resonant inelastic x-ray scattering (RIXS) for tuned for the Cu L edge have shown that energy difference between peak positions near $\mathbf{q} = (\pi, 0)$ and $\mathbf{q} = (\pi/2, \pi/2)$ increases with increasing hole carriers [15, 16]. In fact, the peak energy at $\mathbf{q} = (\pi/2, \pi/2)$ is almost a half of that at $\mathbf{q} = (\pi, 0)$ in the overdoped region [15–18]. It is unclear whether the t - t' - J model can explain this anisotropic behavior, though there are mean-field-type calculations based on random-phase approximation (RPA) for a t - t' - U Hubbard model [17, 18] and QMC simulations for a three-band Hubbard model [19].

In this paper, we investigate both the dynamical spin and charge structure factors in n -leg t - t' - J ladders with totally 96 sites by using dynamical DMRG. With increasing n from $n = 4$ to $n = 8$, the outward dispersion loses its intensity and the energy of the (π, π) excitation decreases, resulting in spectral behavior consistent with INS data for cuprate superconductors [1]. In addition, the energy of the $\mathbf{q} = (\pi, \pi)$ excitation decreases with increasing n . These are accompanied with weakening of charge order in the ground state with increasing n . We also investigate the directional dependence of spin excitation along the $(0, 0)$ - $(\pi, 0)$ and $(0, 0)$ - (π, π) directions using an 8×8 square-lattice cluster. We find an anisotropic behavior along the two directions in terms

* tohyama@rs.tus.ac.jp

of spin excitation energy at the overdoped region, qualitatively consistent with the RIXS data [15, 16], though softening of spin excitation with hole doping is stronger than observed one by RIXS.

This paper is organized as follows. The n -leg t - t' - J ladder with fixed 96 sites ($n = 4, 6, \text{ and } 8$) and dynamical DMRG method are introduced in Sec. II. In Sec. III, we calculate the n dependence of the dynamical spin and charge structure factors around $\mathbf{q} = (\pi, \pi)$ to make clear a relation to stripe charge order. The doping dependence of spin excitation for $n = 8$ around $\mathbf{q} = (\pi, \pi)$ is also shown. In Sec. IV, the directional dependence of the dynamical spin structure factor is examined by using an 8×8 square-shaped cluster. Finally, a summary is given in Sec. V.

II. MODEL AND METHOD

The Hamiltonian of the hole-doped t - t' - J model in two dimensions reads

$$H = -t \sum_{\mathbf{l}, \delta, \sigma} \left(\tilde{c}_{\mathbf{l}+\delta, \sigma}^\dagger \tilde{c}_{\mathbf{l}, \sigma} + \tilde{c}_{\mathbf{l}-\delta, \sigma}^\dagger \tilde{c}_{\mathbf{l}, \sigma} \right) - t' \sum_{\mathbf{l}, \delta', \sigma} \left(\tilde{c}_{\mathbf{l}+\delta', \sigma}^\dagger \tilde{c}_{\mathbf{l}, \sigma} + \tilde{c}_{\mathbf{l}-\delta', \sigma}^\dagger \tilde{c}_{\mathbf{l}, \sigma} \right) + J \sum_{\mathbf{l}, \delta} \left(\mathbf{S}_{\mathbf{l}+\delta} \cdot \mathbf{S}_{\mathbf{l}} - \frac{1}{4} n_{\mathbf{l}+\delta} n_{\mathbf{l}} \right), \quad (1)$$

where t , t' , and J are the nearest-neighbor hopping, the next-nearest-neighbor hopping, and the antiferromagnetic exchange interaction, respectively; $\delta = \mathbf{x}$, \mathbf{y} and $\delta' = \mathbf{x} + \mathbf{y}$, $\mathbf{x} - \mathbf{y}$, with \mathbf{x} and \mathbf{y} being the unit vectors in the x and y directions, respectively; the operator $\tilde{c}_{\mathbf{l}, \sigma} = c_{\mathbf{l}, \sigma} (1 - n_{\mathbf{l}, -\sigma})$, with $n_{\mathbf{l}, \sigma} = c_{\mathbf{l}, \sigma}^\dagger c_{\mathbf{l}, \sigma}$, annihilates a localized electron with spin σ at site \mathbf{l} with the constraint of no double occupancy; $\mathbf{S}_{\mathbf{l}}$ is the spin operator at site \mathbf{l} ; and $n_{\mathbf{l}} = n_{\mathbf{l}, \uparrow} + n_{\mathbf{l}, \downarrow}$. In the following calculations, we fix $J/t = 0.4$ and $t'/t = -0.25$, which are typical values appropriate for cuprates with $t \sim 0.35$ eV.

We use $m \times n = 96$ -site lattices with cylindrical geometry, where the x direction with m sites has an open boundary condition while the y direction with n sites has a periodic boundary condition. We call this lattice the n -leg t - t' - J ladder. We consider three cases: $(m, n) = (24, 4)$, $(16, 6)$, and $(12, 8)$. The hole density for N_h holes in the ladder is defined by $x = N_h/96$. In the $m \times n$ ladder, the y component of momentum \mathbf{q} is determined by using standard translational symmetry, i.e., $q_y = 2n_y\pi/n$ ($n_y = 0, \pm 1, \dots, \pm(n/2 - 1), n/2$), but the x component is given by $q_x = n_x\pi/(m+1)$ ($n_x = 1, 2, \dots, m$) because of the open boundary condition. Defining l_x (l_y) as the x (y) component of site \mathbf{l} , we can write the Fourier component for the z component of spin operator and that of charge operator as

$$S_{\mathbf{q}}^z = \sqrt{\frac{2}{(m+1)m}} \sum_{\mathbf{l}} \sin(q_x l_x) e^{-iq_y l_y} S_{\mathbf{l}}^z, \quad (2)$$

and

$$N_{\mathbf{q}} = \sqrt{\frac{2}{(m+1)m}} \sum_{\mathbf{l}} \sin(q_x l_x) e^{-iq_y l_y} n_{\mathbf{l}}, \quad (3)$$

respectively.

The dynamical spin and charge structure factors, $S(\mathbf{q}, \omega)$ and $N(\mathbf{q}, \omega)$, are defined as

$$S(\mathbf{q}, \omega) = -\frac{1}{\pi} \text{Im} \langle 0 | S_{-\mathbf{q}}^z \frac{1}{\omega - H + E_0 + i\gamma} S_{\mathbf{q}}^z | 0 \rangle, \quad (4)$$

and

$$N(\mathbf{q}, \omega) = -\frac{1}{\pi} \text{Im} \langle 0 | \tilde{N}_{-\mathbf{q}} \frac{1}{\omega - H + E_0 + i\gamma} \tilde{N}_{\mathbf{q}} | 0 \rangle, \quad (5)$$

where $|0\rangle$ represents the ground state with energy E_0 , $\tilde{N}_{\mathbf{q}} = N_{\mathbf{q}} - \langle 0 | N_{\mathbf{q}} | 0 \rangle$, and γ is a small positive number.

We calculate Eqs. (4) and (5) for the $m \times n$ t - t' - J ladder using dynamical DMRG, where we use three kinds of target states: for $S(\mathbf{q}, \omega)$, (i) $|0\rangle$, (ii) $S_{\mathbf{q}}^z |0\rangle$, and (iii) $(\omega - H + E_0 + i\gamma)^{-1} S_{\mathbf{q}}^z |0\rangle$, and for $N(\mathbf{q}, \omega)$ we use $\tilde{N}_{\mathbf{q}}$ instead of $S_{\mathbf{q}}^z$. Target state (iii) is evaluated using a kernel-polynomial expansion method [20], where the Lorentzian broadening γ in Eqs. (4) and (5) is replaced by a Gaussian broadening with a half width at half maximum of $0.08t$. In our numerical calculations of $S(\mathbf{q}, \omega)$, we divide the energy interval $[0, t]$ by 50 mesh points and target all of the points at once.

To perform DMRG for the $m \times n$ t - t' - J ladder, we construct a snakelike one-dimensional chain and use the maximum truncation number $M = 6000$. Resulting truncation error is less than 10^{-3} . To check convergence of our numerical results in terms of m , we performed dynamical DMRG calculations with $M = 4000$ for $n = 8$ and found that, for small x , calculated results are similar to those for $M = 6000$. For large x , the results of $M = 4000$ and $M = 6000$ are not necessarily the same (not shown) even though the difference is limited to a quantitative level. The $M = 6000$ calculation for the $m \times n$ t - t' - J ladder is the best one that we can perform by our present computer resources. More time consuming calculations more than $M = 6000$ remains as a future problem.

For square geometry discussed in Sec. IV, we use an 8×8 t - t' - J cluster with open boundary condition in both directions. In this cluster, we take $M = 8000$ for the calculation of $S(\mathbf{q}, \omega)$.

III. LADDER GEOMETRY OF THE t - t' - J MODEL

A. Effect of the number of leg

We examine the effect of the number of leg n on $S(\mathbf{q}, \omega)$ in the $m \times n = 96$ t - t' - J ladder. Figure 1 shows $S(\mathbf{q}, \omega)$ from $\mathbf{q} = (0.5\pi, \pi)$ to (π, π) for $x = 8/96 = 0.083$ (left

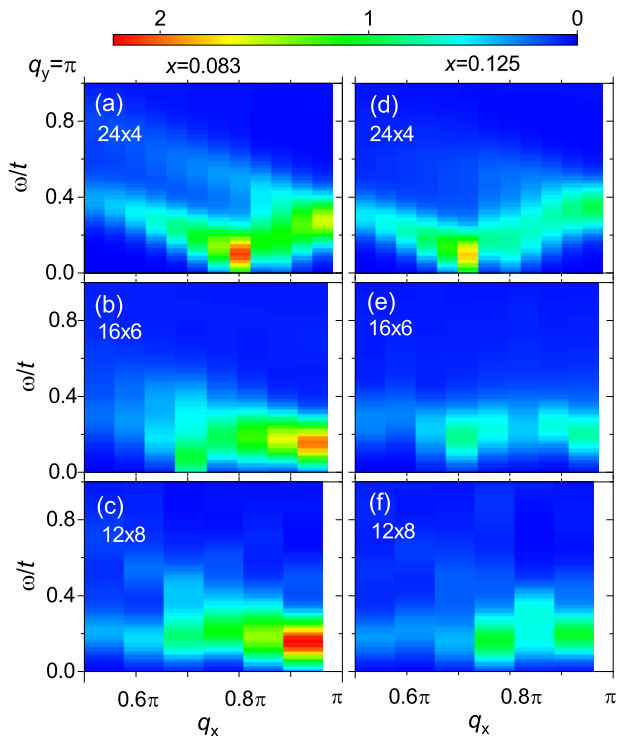


FIG. 1. $S(\mathbf{q}, \omega)$ from $\mathbf{q} = (0.5\pi, \pi)$ to (π, π) in the $m \times n$ t - t' - J ladder with $J/t = 0.4$ and $t'/t = -0.25$. (a) 24×4 , (b) 16×6 , and (c) 12×8 for $x = 0.083$. (d) 24×4 , (e) 16×6 , and (f) 12×8 for $x = 0.125$.

panels) and $x = 12/96 = 0.125$ (right panels). For $n = 4$, there is a low-energy excitation at $q_{IC} = \pi(1 - 2x)$ as shown in Figs. 1(a) and 1(d), which is consistent with incommensurate vectors reported in hole-doped cuprate superconductor $\text{La}_{2-x}\text{Sr}_x\text{CuO}_4$ [21]. This low-energy excitation is originated from the formation of stripe order in the ground state [14]. Linear dispersive branches emerge from q_{IC} toward both the $q_x = \pi$ (inward) and $q_x = 0$ (outward) directions. In the INS experiment [1], the outward dispersion has not been observed. Furthermore, in other calculations of $S(\mathbf{q}, \omega)$ under the stripe order for the 2D extended Hubbard model based on RPA [3] and time-dependent Gutzwiller approximation [5], the outward dispersion loses its intensity quickly for small x . Therefore, the present inconsistency may arise from ladder geometry. In fact, with increasing n from $n = 6$ [Figs. 1(b) and 1(e)] to $n = 8$ [Figs. 1(c) and 1(f)], spectral shape changes significantly. At $x = 0.083$, spectral weight moves toward $q_x = \pi$ and incommensurate low-energy excitation becomes less clear with increasing n . At $x = 0.125$, the outward dispersion around q_{IC} becomes very weak as seen in Figs. 1(e) and 1(f), giving rise to a consistent behavior with the experimental observation.

The energy position of the (π, π) excitation is also dependent on n . At $x = 0.125$, the corresponding position is $\omega/t \sim 0.4$ for $n = 4$ and shifts to the low-energy side with increasing n , resulting in $\omega/t \sim 0.2 = J/2$ [see Fig. 1(f)]. The energy $J/2$ is quantitatively consistent

with experimental observation [1]. Therefore, it would be fair to say that the $n = 8$ result at $x = 0.125$ reasonably reproduces experimental behaviors of spin excitation around $\mathbf{q} = (\pi, \pi)$ observed by INS.

It is interesting to note that spectral distribution at $q_x = 0.85\pi$ for $n = 8$ shown in Fig. 1(f) is slightly higher in energy than that at neighboring q_x . This is similar to the case of $n = 6$ but different from the case of $n = 4$ shown in Fig. 1(d), where the energy at $q_x = 0.85\pi$ is the middle of those at $q_x = q_{IC}$ and $q_x = \pi$. Therefore, the spectral distribution for $n = 8$ at $x = 0.125$ indicates that two contributions at $q_x = q_{IC}$ and $q_x = \pi$ have different origin in contrast to the case of $n = 4$. This supports the idea that there is an upward excitation starting from the (π, π) excitation, i.e., an upper part of hourglass spin excitation, which is independent of the incommensurate low-energy excitation [22].

To understand the change of spin excitation with increasing x , we calculate the hole number $n_h(l_x)$ at the leg position l_x as shown in Figs. 2(a) and 2(b) for $x = 0.083$ and $x = 0.125$, respectively. We note that $n_h(l_x)$ is almost independent of the rung l_y . In the 24×4 lattice, $n(l_x)$ oscillates with period of $1/(2x)$ as a consequence of the formation of stripe order [14]. This x dependence is closely related to incommensurability of spin excitation in the 24×4 lattice. For the 12×8 lattice, oscillation also exists with similar amplitude to the 24×4 lattice, but its oscillation period is not uniform over the lattice. In other words, holes are distributed with oscillating behavior along l_x , but the period is not well-defined. We call this disordered stripe.

To see hole dynamics in the 12×8 lattice, we show $N(\mathbf{q}, \omega)$ along the q_x direction with $q_y = 0$ in Figs. 2(c) and 2(d) for $x = 0.083$ and $x = 0.125$, respectively. Because of disordered stripe, low-energy excitation in $N(\mathbf{q}, \omega)$ is not pronounced at $q_x = 4x\pi$ in contrast to the case of the 24×4 lattice [14]. In particular, we cannot see low-energy excitation at $q_x = 0.5\pi$ for $x = 0.125$ that is a signature of static stripe order seen in $\text{La}_{1.875}\text{Ba}_{0.125}\text{CuO}_4$ [2]. This is a clear indication that static stripe is less stable in the ground state with increasing the number of leg. This contrasting behavior in charge channel between the 24×4 and 12×8 lattices is related to contrasting spin excitation discussed above. It is interesting to note that, even if there is no clear evidence of the 4-lattice period stripe order at $x = 0.125$, low-energy spin excitation near $q_x = 0.75\pi$ is realized in Fig. 1(f). This strongly indicates the contribution of non-static stripe component to incommensurate spin excitation, for example, itinerant component due to quasi-one-dimensional Fermi surface [23].

B. Doping dependence of $S(\mathbf{q}, \omega)$

Figure 3 shows the x dependence of $S(\mathbf{q}, \omega)$ from $\mathbf{q} = (0.5\pi, \pi)$ to (π, π) in the 12×8 t - t' - J ladder. At $x = 0$, dispersive spectral weight follows spin-wave dispersion as

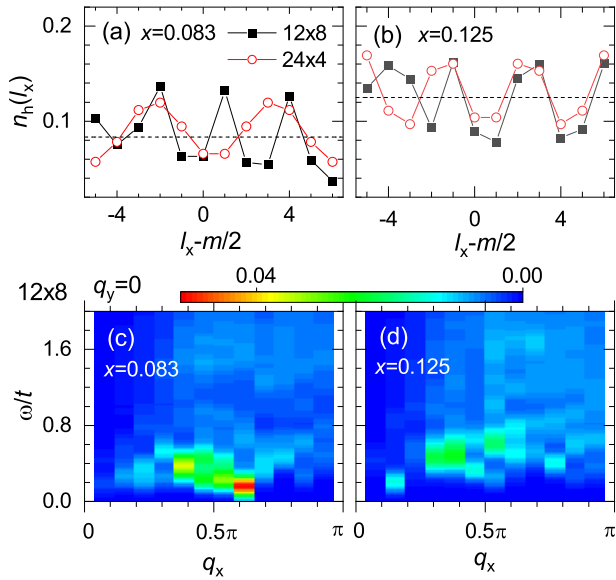


FIG. 2. (a) Hole number $n_h(l_x)$ at the leg position l_x for $x = 0.083$ and (b) that at $x = 0.125$ in the 24×4 ($m = 24$ and red circles) and 12×8 ($m = 12$ and black squares) t - t' - J ladder with $J/t = 0.4$ and $t'/t = -0.25$. $n_h(l_x)$ is obtained by averaging over l_y but the l_y dependence of hole number is very small. The horizontal dotted line denotes averaged hole density x . (c) $N(\mathbf{q}, \omega)$ along q_x with $q_y = 0$ for the 12×8 t - t' - J ladder at $x = 0.083$ and (d) that at $x = 0.125$.

expected. We note that spectral weight near $\mathbf{q} = (\pi, \pi)$ is located slightly below the spin-wave dispersion and that there is a small low-energy weight below the spin-wave energy at $q_x = 0.77\pi$, both of which are due to finite-size effect of the 12×8 cluster.

With increasing x from $x = 0$ to $x = 10/96 = 0.104$ shown in Fig. 3(c), spectral weight near (π, π) decreases and low-energy spectral weight below the spin-wave dispersion spreads to the outward direction from (π, π) . At $x = 0.125$, low-energy excitation with strong intensity at $\mathbf{q} = (0.77\pi, \pi)$ appears as shown in Fig. 3(d). Note that Fig. 3(d) is the same figure as Fig. 1(f) but their color scale is different. With further increasing x , the outward spectral weight is reduced and whole intensity distributes over all momentum region with small intensity.

At $x = 0.167$, the main spectral weight near $\mathbf{q} = (\pi, \pi)$ is located $\omega \sim 0.4J$, whose energy position is higher than that for other x . Taking into account the fact that spectral weight at $q_x = 0.55\pi$ is largest accompanied by broad spectral distribution over whole momentum and energy range, we speculate that itinerant nature dominates spin excitation in the overdoped region as expected.

IV. SQUARE GEOMETRY OF THE t - t' - J MODEL

Recent RIXS experiments have shown the doping dependence of paramagnon excitation [15, 16, 19] and the

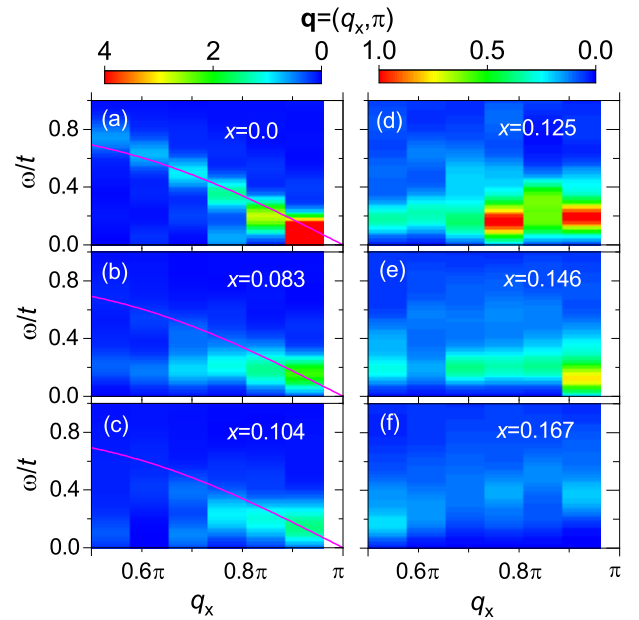


FIG. 3. The x dependence of $S(\mathbf{q}, \omega)$ from $\mathbf{q} = (0.5\pi, \pi)$ to (π, π) in the 12×8 t - t' - J ladder with $J/t = 0.4$ and $t'/t = -0.25$. (a) $x = 0$ (half filling), (b) $x = 4/96 = 0.083$, (c) $x = 8/96 = 0.104$, (d) $x = 12/96 = 0.125$, (e) $14/96 = 0.146$, and (f) $x = 16/96 = 0.167$. The intensity above 4 at $q_x = 0.92\pi$ in (a) is colored in red and the maximum intensity is 1026 at $\omega = 0.064$. The purple line in (a)-(c) represents spin-wave dispersion at half filling obtained by the linear spin-wave theory for the 2D Heisenberg model.

difference of excitation energies along the $(0, 0)$ - $(\pi, 0)$ and $(0, 0)$ - (π, π) directions [15–19]. In order to check whether the t - t' - J model can explain this directional dependence or not, it is necessary to examine non-ladder geometrical systems. We therefore use an 8×8 t - t' - J cluster with open boundary condition.

Before going to spin excitation, we need to clarify the ground state of the cluster within our DMRG calculations. Figure 4 exhibits the doping dependence of hole-density and spin-density distributions. For hole density, we show in Figs. 4(a)-4(d) the deviation of hole number at each site from the average value x , which is defined by $\Delta n_h(l_x, l_y) = 1 - \langle 0 | n_{\mathbf{l}} | 0 \rangle - x$. The doping dependence of the spin density $\langle 0 | S_{\mathbf{l}}^z | 0 \rangle$ at each site is shown in Figs. 4(e)-4(h).

At $x = 4/64 = 0.0625$ [Fig. 4(a)], hole carriers tend to be localized at central region with ordered distribution. This may be partly due to the effect of open boundary condition that pushes holes from the boundaries to the center in order to gain kinetic energy. $\langle 0 | S_{\mathbf{l}}^z | 0 \rangle$ at $x = 0.0625$ [Fig. 4(e)] is uniform and almost zero. At $x = 8/64 = 0.125$ [Fig. 4(b)], $\Delta n_h(l_x, l_y)$ exhibits directional distribution similar to charge stripe. In this case, the y direction is chosen as the direction of charge river in our DMRG procedure. $\langle 0 | S_{\mathbf{l}}^z | 0 \rangle$ in Fig. 4(f) shows antiferromagnetic (ferromagnetic) spin arrangement at hole-rich (hole-poor) region as expected. This spin ar-

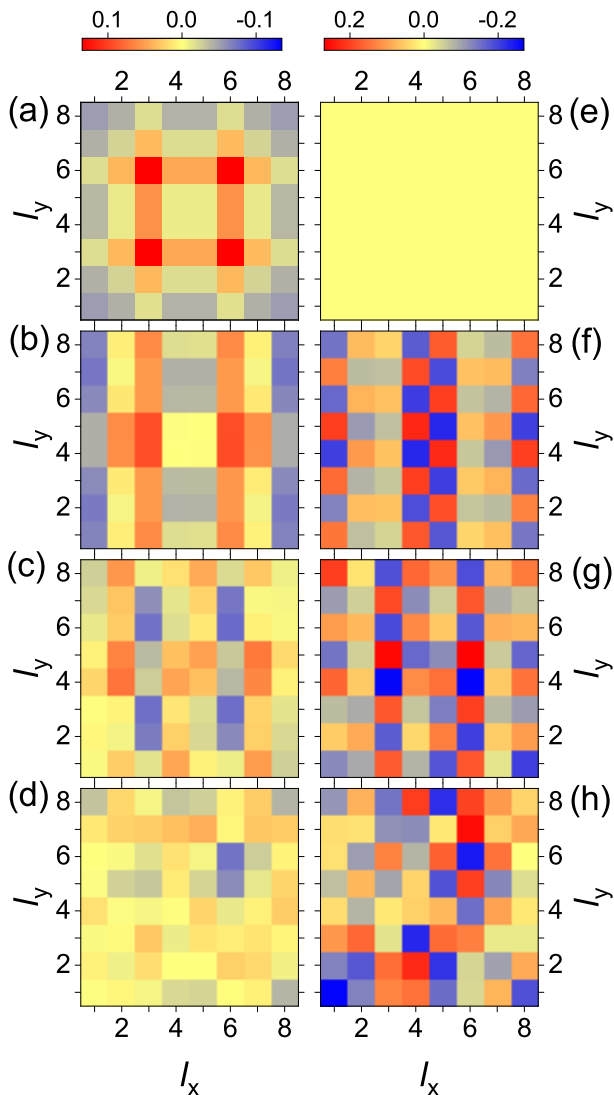


FIG. 4. Site-dependent hole density deviated from average value x , $\Delta n_h(l_x, l_y)$, for the 8×8 t - t' - J cluster with open boundary condition ($J/t = 0.4$ and $t'/t = -0.25$); (a) $x = 0.0625$, (b) $x = 0.125$, (c) $x = 0.1875$, and (d) $x = 0.25$. Each square represents each site and intensity is colored as shown on the top of (a). Site-dependent spin density $\langle 0|S_l^z|0\rangle$; (e) $x = 0.0625$, (f) $x = 0.125$, (g) $x = 0.1875$, and (h) $x = 0.25$. Their intensity is colored as shown on the top of (e).

rangement in the ground state gives rise to low-energy incommensurate spin excitation around $\mathbf{q} = (0.7\pi, \pi)$ (not shown).

With further increasing x , hole distribution becomes more disordered [see Figs. 4(c) and 4(d)] and spin density as well [see Figs. 4(g) and 4(h)]. The non-uniform distribution of hole and spin in our simulation comes from either intrinsic nature of doped Mott insulator or inadequate convergence of our DMRG. We cannot judge the latter from our present computational resources. Nevertheless, high-energy excitation from these ground states will give us intrinsic nature of spin dynamics in doped

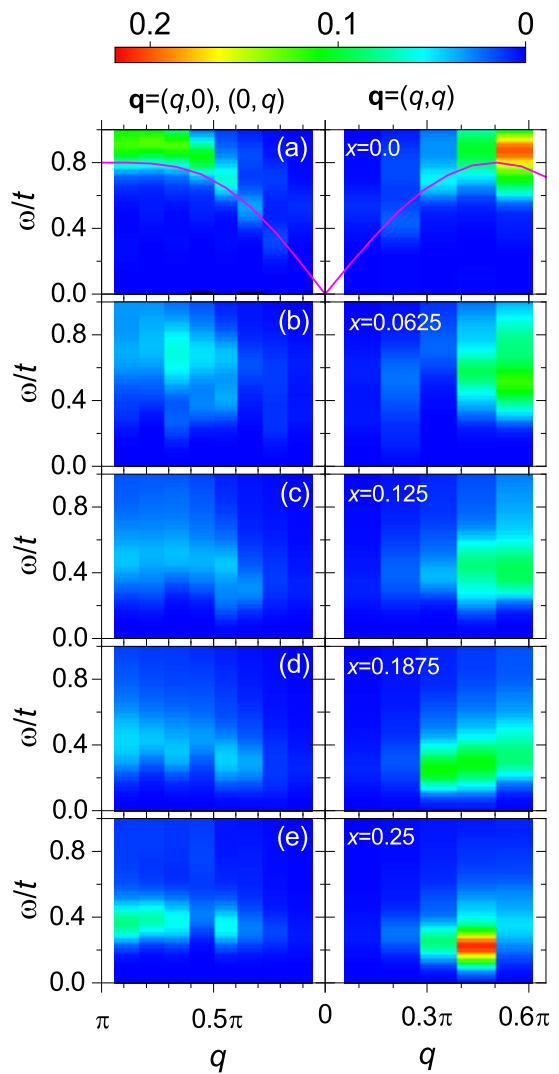


FIG. 5. The x dependence of $S(\mathbf{q}, \omega)$ from $\mathbf{q} = (\pi, 0)$ and $(0, \pi)$ to $(0, 0)$ (left panels) and from $\mathbf{q} = (0, 0)$ to $(0.6\pi, 0.6\pi)$ (right panels) in the 8×8 t - t' - J cluster with open boundary condition ($J/t = 0.4$ and $t'/t = -0.25$). The purple lines in (a) represent spin-wave dispersion at half filling obtained by the linear spin-wave theory for the 2D Heisenberg model.

Mott insulator because of less sensibility of high-energy physics to small difference of ground-state properties. In this sense, a part of intrinsic nature on directional spin excitation at the high energy region measured by RIXS would be captured by our 8×8 t - t' - J cluster.

Figure 5 shows the doping dependence of $S(\mathbf{q}, \omega)$ from $\mathbf{q} = (\pi, 0)$ and $(0, \pi)$ to $(0, 0)$ (left panels) and from $\mathbf{q} = (0, 0)$ to $(0.6\pi, 0.6\pi)$ (right panels) in the 8×8 t - t' - J cluster. For the $(0, 0)$ - $(\pi, 0)$ and $(0, 0)$ - $(0, \pi)$ directions, averaged spectral weight $[S((q, 0), \omega) + S((0, q), \omega)]/2$ is plotted. At $x = 0$, the lowest-energy excitation follows spin-wave dispersion as seen in Fig. 5(a) and spectral weights are distributed in the same energy region in both the directions. With increasing x , their intensity reduces accompanied by the shift of spectral weight toward lower

energy. At $x = 0.25$, main spectral weight near $\mathbf{q} = (\pi, 0)$ and $(0, \pi)$ is located around $\omega \sim 0.4t = J$, while that near $\mathbf{q} = (\pi/2, \pi/2)$ is located around $\omega \sim 0.2t = J/2$. This asymmetry is consistent with recent observation for the overdoped region of cuprates in RIXS [15, 16], although the calculated spectral weight is located lower in energy than the observed ones. For more quantitative comparison, we need to include correlated hopping terms related to three sites [24] and/or return to original Hubbard-type models [19].

V. SUMMARY

In summary, we have investigated the dynamical spin and charge structure factors, $S(\mathbf{q}, \omega)$ and $N(\mathbf{q}, \omega)$, in the $m \times n$ t - t' - J ladder keeping $m \times n = 96$ sites. We have used dynamical DMRG for their calculations. With increasing n from $n = 4$ (four-leg ladder) to $n = 8$ (eight-leg ladder), we found that strong outward dispersion from the incommensurate position toward $\mathbf{q} = (0, \pi)$, which has been reported before for $n = 4$ [14], loses its intensity followed by the decrease of excitation energy at $\mathbf{q} = (\pi, \pi)$. This leads to spectral behaviors consistent with INS data for cuprate superconductors [1], indicating the crucial role of increasing number of leg in our model. We found that the increase of n changes the ground-state charge distribution from ordered stripe to disordered one.

For a fully squared system, we have examined the 8×8 t - t' - J lattice with open boundary condition. Even in this system, hole carriers distribute inhomogeneously in the

ground state. Examining the dependence of spin excitation along the $(0, 0)$ - $(\pi, 0)$ and $(0, 0)$ - (π, π) directions, we found an anisotropic behavior along the two directions in spin excitation at the overdoped region. This is qualitatively consistent with recent RIXS data [15, 16], although softening of spin excitation with hole doping is stronger than observed one. The anisotropic behavior realized in the high-energy region at large \mathbf{q} is expected to be insensitive to the inhomogeneous charge distribution in the ground state. To confirm this statement, it is necessary to perform more large-scale DMRG calculation, which remains to be a future problem.

ACKNOWLEDGMENTS

We thank M. Mori and M. Fujita for fruitful discussions. This work was supported by MEXT, Japan, as a social and scientific priority issue (creation of new functional devices and high-performance materials to support next-generation industries) to be tackled by using a post-K computer, by MEXT HPCI Strategic Programs for Innovative Research (SPIRE; hp190023), and by the interuniversity cooperative research program of IMR, Tohoku University. The numerical calculation was carried out at the K Computer and HOKUSAI, RIKEN Advanced Institute for Computational Science, and the facilities of the Supercomputer Center, Institute for Solid State Physics, University of Tokyo. This work was also supported by the Japan Society for the Promotion of Science, KAKENHI (Grants No. 19H01829 and No. JP19H05825).

-
- [1] For a recent review, see M. Fujita, H. Hiraka, M. Mitsuhashi, M. Matsuura, J. M. Tranquada, S. Wakimoto, G. Xu, and K. Yamada, *J. Phys. Soc. Jpn.* **81**, 011007 (2012) and references therein.
 - [2] J. M. Tranquada, B. J. Sternlieb, J. D. Axe, Y. Nakamura, and S. Uchida, *Nature (London)* **375**, 561 (1995).
 - [3] E. Kaneshita, M. Ichioka, and K. Machida, *J. Phys. Soc. Jpn.* **70**, 866 (2001).
 - [4] G. Seibold and J. Lorenzana, *Phys. Rev. Lett.* **94**, 107006 (2005).
 - [5] G. Seibold and J. Lorenzana, *Phys. Rev. B* **73**, 144515 (2006).
 - [6] F. Krüger and S. Scheidl, *Phys. Rev. B* **67**, 134512 (2003).
 - [7] E. W. Carlson, D. X. Yao, and D. K. Campbell, *Phys. Rev. B* **70**, 064505 (2004).
 - [8] E. W. Huang, C. B. Mendl, S. Liu, S. Johnston, H.-C. Jiang, B. Moritz, and T. P. Devereaux, *Science* **358**, 1161 (2017).
 - [9] E. W. Huang, C. B. Mendl, H.-C. Jiang, B. Moritz, and T. P. Devereaux, *npj Quantum Materials* **3**, 22 (2018).
 - [10] T. Tohyama, C. Gazza, C. T. Shih, Y. C. Chen, T. K. Lee, S. Maekawa, and E. Dagotto, *Phys. Rev. B* **59**, R11649 (1999).
 - [11] S. R. White and D. J. Scalapino, *Phys. Rev. B* **60**, R753 (1999).
 - [12] D. J. Scalapino and S. R. White, *Physica C* **481**, 146 (2012).
 - [13] J. F. Dodaro, H.-C. Jiang, and S. A. Kivelson, *Phys. Rev. B* **95**, 155116 (2017).
 - [14] T. Tohyama, M. Mori, and S. Sota, *Phys. Rev. B* **97**, 235137 (2018).
 - [15] D. Meyers, H. Miao, A. C. Walters, V. Bisogni, R. S. Springell, M. d'Astuto, M. Dantz, J. Pellicciari, H. Y. Huang, J. Okamoto, D. J. Huang, J. P. Hill, X. He, I. Božović, T. Schmitt, and M. P. M. Dean *Phys. Rev. B* **95**, 075139 (2017).
 - [16] H. C. Robarts, M. Barthélemy, K. Kummer, M. García-Fernández, J. Li, A. Nag, A. C. Walters, K. J. Zhou, and S. M. Hayden, *Phys. Rev. B* **100**, 214510 (2019).
 - [17] M. Guarise, B. Dalla Piazza, H. Berger, E. Giannini, T. Schmitt, H. M. Rønnow, G. A. Sawatzky, J. van den Brink, D. Altenfeld, I. Eremin, and M. Grioni, *Nat. Commun.* **5**, 5760 (2014).
 - [18] C. Monney, T. Schmitt, C. E. Matt, J. Mesot, V. N. Strocov, O. J. Lipscombe, S. M. Hayden, and J. Chang, *Phys. Rev. B* **93**, 075103 (2016).
 - [19] Y. Y. Peng, E. W. Huang, R. Fumagalli, M. Minola, Y.

- Wang, X. Sun, Y. Ding, K. Kummer, X. J. Zhou, N. B. Brookes, B. Moritz, L. Braicovich, T. P. Devereaux, and G. Ghiringhelli, *Phys. Rev. B* **98**, 144507 (2019).
- [20] S. Sota and T. Tohyama, *Phys. Rev. B* **82**, 195130 (2010).
- [21] K. Yamada, C. H. Lee, K. Kurahashi, J. Wada, S. Wakimoto, S. Ueki, H. Kimura, Y. Endoh, S. Hosoya, G. Shirane, R. J. Birgeneau, M. Greven, M. A. Kastner, and Y. J. Kim, *Phys. Rev. B* **57**, 6165 (1998).
- [22] M. Fujita, private communication.
- [23] H. Yamase and H. Kohno, *J. Phys. Soc. Jpn.* **70**, 2733 (2001).
- [24] C. J. Jia, E.A. Nowadnick, K. Wohlfeld, Y.F. Kung, C.-C. Chen, S. Johnston, T. Tohyama, B. Moritz, and T.P. Devereaux, *Nat. Commun.* **5**, 3314 (2014).